

ARTICLES

How the Central Torsion Angle Affects the Rates of Nonradiative Decay in Some Geometrically Restricted *p*-Quaterphenyls

Ben D. Allen, Andrew C. Benniston, Anthony Harriman,* Irantzu Llarena, and Craig A. Sams

Molecular Photonics Laboratory, Bedson Building, School of Natural Sciences, Newcastle University, Newcastle upon Tyne NE1 7RU, U.K.

Received: October 24, 2006; In Final Form: February 8, 2007

A small series of *p*-quaterphenyl derivatives has been prepared in which the dihedral angle (ϕ) for the two central rings is constrained by dialkoxy spacers of varying length. The photophysical properties of these compounds remain comparable, but there is a clear correlation between the rate constants for nonradiative decay of both singlet and triplet excited states and ϕ in fluid solution. The rates tend toward a minimum as ϕ approaches 90° . These effects are attributed to the general phenomenon of extended delocalization and can be traced to a combination of changes in the Huang–Rhys factor and the electron–vibrational coupling matrix element, both relating to displacement of the relevant potential energy surfaces and to the medium-frequency vibronic mode coupled to decay. The latter effect arises because of different levels of conjugation in the ground-state molecule. Such findings might have important implications for the design of improved light-emitting diodes. A similar angle dependence is noted for the yield of the π -radical cation formed on photoionization in a polar solvent, but here, the effect is due to variations in the respective energy gaps between the relevant excited states.

Introduction

Research into conducting polymers continues to thrive as the list of potential applications grows ever longer. One of many interesting features of such materials concerns the conjugation length,¹ as this property helps to control the photophysics and, in particular, the emission wavelength. For poly(aryl)-based materials, it has been reported² that the conjugation length for the singlet excited state is restricted to about 10 repeat units because of conformational effects. Other studies³ show an incremental change in emission wavelength with increasing degree of oligomerization, but in reality, the effect is extremely small after the repeat length reaches double figures. The conjugation length for the corresponding triplet state, on the other hand, is often restricted to a single repeat unit, at least for

poly(thiophene)-based materials.⁴ It has been stressed that the conjugation length,⁵ or the degree of electron delocalization,⁶ depends markedly on the molecular conformation and, most importantly, on the mutual alignment of adjacent aromatic residues. Molecular conductivity is believed to be at a maximum when neighboring aromatic units adopt a coplanar arrangement,⁷ and it is the disruption of this planarity that controls the conjugation length for singlet excited states.⁸ The same situation abounds when the repeat unit comprises ethynylated aromatic functions.⁹ Systematic evaluation of this structural effect, and especially of how molecular conductivity depends on the dihedral angle between proximal aryl rings,^{10,11} is a major challenge that requires access to appropriate model compounds in which the geometry can be changed in a regular manner. We recently introduced a concept whereby the dihedral angle around a central biphenyl unit can be controlled by the length

* Corresponding author. E-mail: Anthony.harriman@ncl.ac.uk.

of a tethering strap¹² and applied this approach to the study of intramolecular electron transfer,¹³ triplet energy transfer,¹⁴ and vibrational perturbation of excited-state decay.¹⁵ A related approach has been used here to examine the effects of a change in central dihedral angle on the photophysical properties of *p*-quaterphenyl derivatives. The intention is to expose any systematic variation in the conjugation length as the dihedral angle is varied. A main point of interest for the present study, unlike our previous work carried out with strapped biphenyls, is that the molecular geometry is likely to depend on the state of excitation. In this respect, it should be recalled that early studies by Berlman¹⁶ used simple traits of absorption and fluorescence spectral profiles to infer the planarity of ground and excited states for multi-ring aromatics.

The photophysical behavior of the linear aromatic *p*-quaterphenyl (*p*-QT) is well-known;¹⁶ this is a molecule that has been studied widely and that has found many applications in such areas as nonlinear optics,¹⁷ liquid crystals,¹⁸ and laser dyes.¹⁹ The compound displays relatively intense fluorescence in fluid solution that is known to originate from the long-axis $^1L_a \rightarrow ^1A$ transition. Interestingly, Taber²⁰ showed in 1965 that the scintillator efficiency for *p*-QT could be controlled by altering the planarity of the external rings in the molecule. Subsequently, Daub et al.²¹ prepared other constrained derivatives, but no systematic study of their electronic behavior was made. We envisaged that derivatives QT1–QT4 would be useful candidates with which to explore the question of whether the central angle controls the extent of electronic communication along the molecular axis, as this angle can be varied by changing the length of the tether. The simplicity of these molecular structures makes them suitable for computational studies.

Experimental Section

Methods. All chemicals were purchased from commercial sources and were used as received. Solvents were dried by standard literature methods²² before being distilled and stored under nitrogen over 4-Å molecular sieves. ¹H and ¹³C NMR spectra were recorded with JEOL Lambda 500 MHz and Bruker AVANCE 300 MHz spectrometers. Routine mass spectra and elemental analyses were obtained using in-house facilities. Absorption spectra were recorded with a Hitachi U3310 spectrometer, and fully corrected fluorescence spectra were recorded with a Yvon-Jobin Fluorolog tau-3 spectrophotometer. All fluorescence measurements were made using optically dilute solutions and were corrected for spectral imperfections of the instrument by reference to a standard lamp. Fluorescence quantum yields were recorded relative to 9,10-diphenylanthracene in deoxygenated cyclohexane.²³ Low-temperature studies were performed with quartz tubes housed in an immersion-well Dewar filled with liquid N₂. Phosphorescence studies were conducted using a Hitachi F4500 spectrofluorimeter equipped with an optical shutter to remove prompt fluorescence, and lifetimes were measured with a PTI Xenoflash instrument. Time-resolved fluorescence measurements were made by time-correlated, single photon counting using a PTI EasyLife spectrophotometer. Excitation was effected at 290 nm using a fast laser diode (fwhm = 500 ps), and fluorescence was isolated from scattered light using rejection filters. After deconvolution, the temporal resolution of this setup was about 400 ps. Laser flash photolysis studies were performed with an Applied Photophysics LKS.60 spectrometer. Excitation was provided with a frequency-quadrupled, Q-switched Nd:YAG laser ($\lambda = 266$ nm, fwhm = 4 ns). Transient differential absorption spectra were recorded point-by-point, and decay kinetics were measured

at various detection wavelengths and signal-averaged. Solutions were thoroughly purged with N₂ before each experiment. Where necessary, the laser intensity was adjusted using crossed polarizers.

Computational studies were performed using the GAMESS²⁴ and Gaussian 03²⁵ programs. All energy-related calculations employed the 6-31g* basis set and were done in vacuo. Ground-state geometries were determined using the B3LYP hybrid DFT method in GAMESS. In each case, confirmation of an energy minimum was provided by determining vibrational frequencies. Excited-state structures were calculated by the CIS method²⁶ in GAMESS, with a total of two singlet states calculated during the CIS step. This was done to ensure that there was no interference between closely spaced, excited-state levels. Second derivatives were not calculated for the excited-state structures because of computational cost, and it therefore cannot be confirmed that the reported geometries are genuine minima. However, the general trend toward planarity for the calculated geometries agrees well with previous studies on the parent *p*-quaterphenyl.²⁷ Cation geometries were also calculated using GAMESS and unrestricted B3LYP,²⁸ whereas T₁ geometries were determined using the Gaussian 03 UB3LYP²⁹ method. It should be noted that the B3LYP functionals in GAMESS and Gaussian differ. However, whereas the single-point energies differ between the two programs when B3LYP is used, test calculations showed that optimized geometries for each compound were in excellent agreement. Therefore, for consistency, all reported energies were calculated using Gaussian 03, with the structure coming from either a Gaussian or a GAMESS calculation as described above. Time-dependent DFT (TD-DFT) calculations using Gaussian 03 and the B3LYP functional were used to determine excitation energies for all structures considered. This was done because, although it is known that the simple CIS method generally gives good results for geometry optimizations,³⁰ absolute and relative excitation energies are likely to be overestimated.³¹ TD-DFT³² performs much better in this respect, but the lack of TD-DFT analytic gradients in the programs available to us precluded their use for the geometry optimizations. No symmetry restrictions were applied during the calculations.

Materials. Preparation of 3,9-diiodo-5,7-dioxa-dibenzo[*a,c*]cycloheptene (**1**), 3,10-diiodo-6,7-dihydro-5,8-dioxa-dibenzo[*a,c*]cyclooctane, (**2**) 3,11-diiodo-7,8-dihydro-5,9 dibenzo[*a,c*]cyclononane (**3**), and 3,12-diiodo-6,7,8,9-tetrahydro-5,10-dioxa-dibenzo[*a,c*]cyclodecene (**4**) has been described previously.³³

*Preparation of 3,9-Diphenyl-5,7-dioxa-dibenzo[*a,c*]cycloheptane (QT1).* Into a 100-mL three-neck round-bottom flask was added 3,9-diiodo-5,7-dioxa-dibenzo[*a,c*]cycloheptene (250 mg, 0.55 mmol) and dry, N₂-purged toluene (20 mL). Phenyl boronic acid (20 mg, 1.66 mmol) dissolved in a minimal amount of degassed ethanol (5 mL) was added, along with Pd(PPh₃)₄ (20 mg) and 10 mL of Na₂CO₃ (2 M). The mixture was stirred for 30 min under N₂ at room temperature and finally refluxed for 6 h. During this time, the reaction mixture changed from yellow to brown. The mixture was cooled to room temperature, and water was added. The aqueous layer was extracted several times with ethyl acetate. The combined organics were dried over MgSO₄, filtered, and evaporated to afford the crude product, which was purified by column chromatography on silica gel using petroleum ether/dichloromethane (4:1) as the eluant to yield a white solid (150 mg, 0.43 mmol, 78%). ¹H NMR (300 MHz, CDCl₃) $\delta = 7.84$ – 7.87 (d, 2H, $J = 8.3$ Hz), 7.65 – 7.67 (d, 4H, $J = 7.1$ Hz), 7.45 – 7.50 (m, 6H), 7.36 – 7.42 (m, 4H), 5.68 (s, 2H). ¹³C NMR (CDCl₃) $\delta = 98.0, 119.54, 123.1, 126.5,$

127.3, 128.1, 129.2, 129.3, 140.0, 142.1, 156.6. EI-MS calcd for M^+ 350.130, found m/z 350.1317 for $C_{25}H_{18}O_2$. Mp 140–142 °C.

Preparation of 3,10-Diphenyl-6,7-dihydro-5,8-dioxa-dibenzo[*a,c*]cyclooctene (QT2). A procedure similar to the above was used, with 3,10-diiodo-6,7-dihydro-5,8-dioxa-dibenzo[*a,c*]cyclooctane (500 mg, 1 mmol), phenyl boronic acid (40 mg, 3 mmol), Pd(PPh₃)₄ (20 mg), and Na₂CO₃ (2 M, 10 mL). Purification: column chromatography, silica gel, petroleum ether/ethyl acetate (9:1) eluant. Recrystallization from petroleum ether. Yield: 100 mg, 0.27 mmol, 38%, white solid. ¹H NMR (300 MHz, CDCl₃) δ = 7.64–7.67 (d, 4H, *J* = 7.8 Hz), 7.43–7.50 (m, 10H), 7.35–7.41 (m, 2H), 4.52 (m, 2H), 4.18 (m, 2H). ¹³C NMR (CDCl₃) δ = 73.44, 121.5, 123.6, 127.4, 128.0, 129.2, 130.8, 123.2, 140.6, 143.2, 158.6. EI-MS calcd for M^+ 364.1463, found 364.1472 for $C_{26}H_{20}O_2$. Mp 183–186 °C.

Preparation of 3,11-Diphenyl-7,8-dihydro-5,9-dioxa-dibenzo[*a,c*]cyclononene (QT3). A procedure similar to the above was used, with 3,11-diiodo-7,8-dihydro-5,9-dibenzo[*a,c*]cyclononane (200 mg, 0.42 mmol), phenyl boronic acid (0.16 mg, 1.26 mmol), Pd(PPh₃)₄ (20 mg), and Na₂CO₃ (2 M, 10 mL). Purification: column chromatography, silica gel, petroleum ether/dichloromethane (2:1) eluant. Recrystallization from petroleum ether. Yield: 120 mg, 0.3 mmol, 75%, white solid. ¹H NMR (300 MHz, CDCl₃) δ = 7.64–7.66 (d, 4H, *J* = 8.3 Hz), 7.45–7.50 (dd, 4H, *J* = 7.1 Hz, *J'* = 1.8 Hz), 7.36–7.40 (m, 8H), 4.38 (t, 4H, *J* = 5.1 Hz), 2.08 (m, 2H). ¹³C NMR (CDCl₃) δ = 66.3, 71.7, 117.1, 122.4, 127.5, 127.8, 129.2, 130.6, 130.9, 141.2, 142.5, 157.9. EI-MS calcd for M^+ 378.1619, found 378.1619 for $C_{27}H_{22}O_2$. Mp 198–200 °C.

Preparation of 3,12-Diphenyl-6,7,8,9-tetrahydro-5,10-dioxa-dibenzo[*a,c*]cyclododecene (QT4). A procedure similar to the above was used, with 3,12-diiodo-6,7,8,9-tetrahydro-5,10-dioxa-dibenzo[*a,c*]cyclododecene (300 mg, 0.61 mmol), phenyl boronic acid (0.23 mg, 1.80 mmol), Pd(PPh₃)₄ (20 mg), and Na₂CO₃ (2 M, 10 mL). Purification: column chromatography, silica gel, petroleum ether/dichloromethane (2:1) eluant. Recrystallization from petroleum ether. Yield: 150 mg, 0.38 mmol, 62%, white solid. ¹H NMR (300 MHz, CDCl₃) δ = 7.62–7.65 (d, 4H, *J* = 7.1 Hz), 7.43–7.49 (m, 4H), 7.28–7.41 (m, 8H), 4.57 (m, 2H), 4.32 (m, 2H), 2.19 (m, 4H). ¹³C NMR (CDCl₃) δ = 27.8, 71.6, 115.0, 121.2, 127.6, 127.8, 128.5, 129.1, 131.8, 141.5, 142.2, 157.8. EI-MS calcd for M^+ 392.1776 found 392.1784 for $C_{28}H_{24}O_2$. Mp 176–178 °C.

Results and Discussion

Synthesis. Using a multistep synthetic approach, Daub et al.²¹ prepared **QT1–QT4** from 2',3'-dihydroxy-*p*-quaterphenyl by cyclization with dihaloalkanes, but NMR data were not reported for the final compounds. We decided to use an alternative approach that relied on initial construction of the strapped central portion, followed by cross-coupling to attach the terminal phenyl groups. The molecular formulas of the final compounds are shown in Figure 1. The required di-iodo derivatives **1–4** were developed previously¹² and coupled to phenyl boronic acid using standard Suzuki conditions³⁴ to afford the desired derivatives in nonoptimized yields ranging from 38% to 78%. The title compounds could be prepared readily on the 100–150-mg scale. ¹H NMR spectra of the derivatives in CDCl₃ display a number of overlapping resonances in the aromatic region that make complete peak assignment difficult. In comparison, each of the ¹³C{¹H} NMR spectra contain 10 peaks in the aromatic region as expected for symmetric structures. The derivatives **QT1** and **QT3** are readily soluble in chlorinated solvents, whereas **QT2**

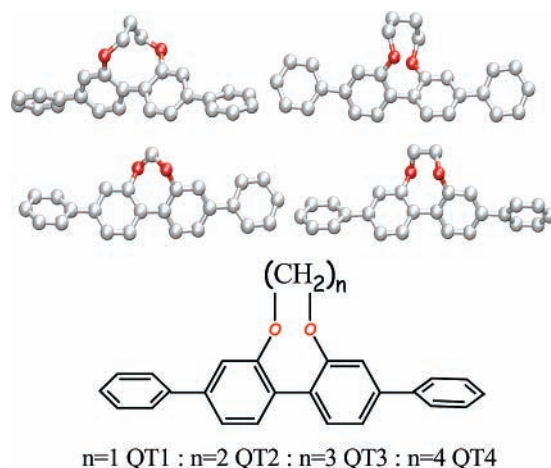


Figure 1. Molecular formulas and energy-minimized conformations of the compounds studied herein.

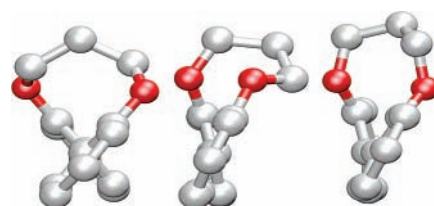


Figure 2. Computed energy-minimized structures for QT3 showing the ground state (left), the first-excited singlet state (center), and the lowest-energy triplet state (right).

and **QT4** are only sparingly soluble. The compounds are stable over prolonged storage, even under ambient lighting, and resistant to photodegradation during laser photolysis in the absence of molecular oxygen.

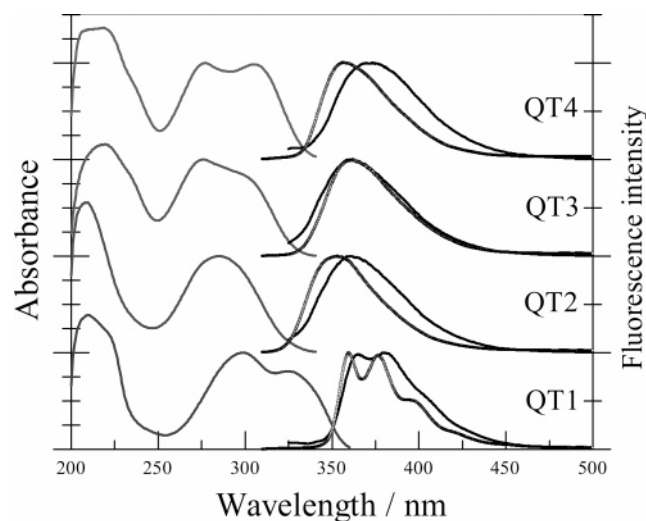
Molecular Modeling. The length of the attached tether is expected to alter the dihedral angle (ϕ) around the central biphenyl unit, at least for the lowest-energy conformations. A secondary effect of the tether, especially the shorter versions, might be to distort the *p*-QP axis from linear to a “banana-like” structure. This latter feature can be represented in terms of the “bend” angle (see Supporting Information). As might be expected from previous studies,^{12–15} changes in the length of the tether lead to a reasonable variation in the dihedral angle (Table 1), with QT3 displaying the largest ϕ value. Increasing the tether beyond a certain length has the effect of reducing ϕ , although it has to be accepted that multiple conformations are possible for the longer straps. There are also modest changes in the bend angle (Table 1), again with QT3 showing the maximum amount of structural distortion. These geometry changes represent a balance between accommodation of the bulky tether, especially the connecting oxygen atoms, and the drive toward planarity for the polycycle. For the parent compound, the four phenyl rings are free to rotate in fluid solution,³⁵ but low-temperature X-ray data³⁶ reveal that the torsion angle between an external and an internal ring is 17.1°, whereas the mean torsion angle between the two internal rings is greater at 22.7°. In solution, the torsion angles are larger, and studies³⁷ indicate average ϕ values of around 37°.

Table 1 also includes the derived ϕ values and bend angles for the first-excited singlet (S_1) states, as calculated by CIS methods.²⁶ Although it is clear that the tether prevents adoption of a planar geometry at the S_1 level, as appears to happen for the parent molecule,¹⁶ there seems to be a general move toward a dihedral angle of ca. 34° (Table 1). The corresponding bend angles are smaller than those found for the corresponding ground

TABLE 1: Compilation of the Important Structural and Energy Data Derived from the Quantum Chemical Computations Made for the Energy-Minimized Geometries in Vacuo

parameter	QT1	QT2	QT3	QT4
ϕ (S_0) (deg)	39.5	53.2	80.6	60.3
ϕ (S_1) (deg)	29.1	37.9	32.1	36.5
ϕ (T_1) (deg)	25.2	33.6	30.1	31.7
bend (S_0) (deg)	6.3	3.8	13.7	8.8
bend (S_1) (deg)	2.3	2.2	6.7	5.6
bend (T_1) (deg)	1.4	4.8	8.5	8.6
E_S^a (eV)	3.99	4.17	4.22	4.40
E_S^b (eV)	3.50	3.41	3.33	3.15
E_T^c (eV)	2.15	2.19	2.05	1.99
IP ^d (eV)	6.55	6.49	6.43	6.27

^a Calculated for the optimized ground-state geometry. ^b Calculated for the optimized S_1 geometry. ^c Calculated for the optimized T_1 geometry. ^d Ionization potential calculated for the optimized cation geometry.

**Figure 3.** Absorption and fluorescence spectra recorded in ethanol solution at room temperature and fluorescence spectra recorded in a glassy ethanol matrix at 77 K.

state, and there is an obvious attempt to seek a linear geometry upon excitation. The ϕ values are considered as representative of the best compromise between reaching a planar geometry but also accommodating the tether.¹² It is notable that **QT1** does not undergo a major structural change upon promotion to the S_1 state. The other compounds experience more pronounced changes in geometry upon excitation, and it is notable that the conformation of the tether alters markedly during this process, as illustrated in Figure 2 for **QT3**. Interestingly, similar calculations for the lowest-energy triplet state give quite comparable angles for T_1 . In each case, the energy-minimized T_1 angle is slightly less than that found for S_1 and considerably different from that found for the ground state (Table 1). There is a corresponding reduction in the computed bend angles. As with S_1 , the triplet state tries to attain a planar geometry.

Photophysical Properties. The absorption spectra for **QT1–QT4** recorded in ethanol solution at room temperature are shown in Figure 3. As also found for *p*-QP,¹⁶ each compound exhibits an intense absorption transition centered at around 210 nm and a weaker transition at about 310 nm. The higher-energy band can be assigned as a $^1A \rightarrow ^1B_b$ transition, whereas the lower-energy band is attributed to the $^1A \rightarrow ^1L_a$ transition.³⁸ There is, in addition, a much less intense $^1A \rightarrow ^1L_b$ transition³⁸ that is hidden beneath the latter band. Each of the main transitions is split into two peaks in the tethered derivatives because of a

TABLE 2: Compilation of the Photophysical Properties Recorded for the Various Compounds in Deoxygenated Ethanol at Room Temperature

parameter	QT1	QT2	QT3	QT4
Δ_{SS} (cm^{-1})	3700	5980	6655	5690
ϕ_F	0.56	0.67	0.75	0.72
τ_S (ns)	0.88	1.00	1.25	1.14
k_{RAD} (10^8 s^{-1})	6.4	6.7	6.0	6.3
τ_T (μs)	4.9	6.4	8.4	7.1
τ_P^a (ms)	4.4	4.5	4.3	4.6
λ_P^a (nm)	470	475	500	500
k_{NR} (10^8 s^{-1})	5.0	3.3	2.0	2.5
k_T (10^5 s^{-1})	2.1	1.6	1.2	1.4
ϕ_{CAT}^b	0.008	0.010	0.021	0.016

^a Recorded at 77 K. ^b Measured in deoxygenated acetonitrile at room temperature.

break in symmetry that destroys the accidental degeneracy inherent to the parent. The actual amount of splitting depends on the length of the tether and is minimal for **QT2** but quite pronounced for **QT4**. Fluorescence is readily observed for each compound in ethanol at room temperature (Figure 3). The spectral profiles and peak positions are insensitive to excitation wavelength, and in each case, there is excellent agreement between corrected excitation spectrum and the corresponding absorption spectrum. The effective Stokes shift (Δ_{SS}) is rather high, being in excess of 3000 cm^{-1} at room temperature, reflecting a change in geometry upon promotion to the S_1 state (Table 2). This finding seems to be in agreement with the results of the computational studies. Indeed, there is a rough correlation between the experimental Stokes shift and the computed difference in ϕ for the ground and S_1 states. It is notable that vibrational fine structure can be observed in the fluorescence spectrum only in the case of **QT1**; in all other cases, the emission band appears as a broad, featureless transition with an indistinct maximum. The spectra remain remarkably similar in a glassy ethanol matrix at 77 K, but the peak maximum undergoes a small blue shift (Figure 3). The fine structure becomes more pronounced for **QT1** at 77 K. Fluorescence polarization studies were performed with the tethered compounds embedded in stretched polyethylene films where it was noted that, in each case, polarization is aligned along the long axis of the molecule.

Fluorescence quantum yields (ϕ_F) were measured in deoxygenated ethanol at room temperature and are seen to be rather high (Table 2). Even so, there is a significant variation across the series. The fluorescence lifetimes (τ_S) are close to 1 ns and also show a dependence on strap length. These generic properties, high ϕ_F and short τ_S , are typical of S_1 states exhibiting considerable 1L_a character.³⁹ The radiative rate constants (k_{RAD}) are relatively high, as expected for such excited states. Low-temperature phosphorescence could be detected with a maximum (λ_P) at ca. 470 nm in each case and a lifetime (τ_P) of ca. 4 ms in deoxygenated ethanol at 77 K (Table 2). The triplet lifetime and triplet energy recorded under these conditions remain fairly insensitive to the nature of the tether. As found for the fluorescence spectra, **QT1** shows structured phosphorescence, but the other derivatives exhibit broad, featureless phosphorescence spectra. The phosphorescence yield was extremely low but could be increased substantially by the addition of iodoethane (10% v/v), in which case τ_P decreased to ca. 1 ms.

The fluorescence properties are not dissimilar from what might be expected for *p*-quaterphenyl derivatives and, in fact, remain comparable to those of *p*-QP ($\phi_F = 0.74$, $\tau_S = 0.8 \text{ ns}$) and terphenyl ($\phi_F = 0.77$, $\tau_S = 0.95 \text{ ns}$). The computational studies account for the observed trend in excitation energies,

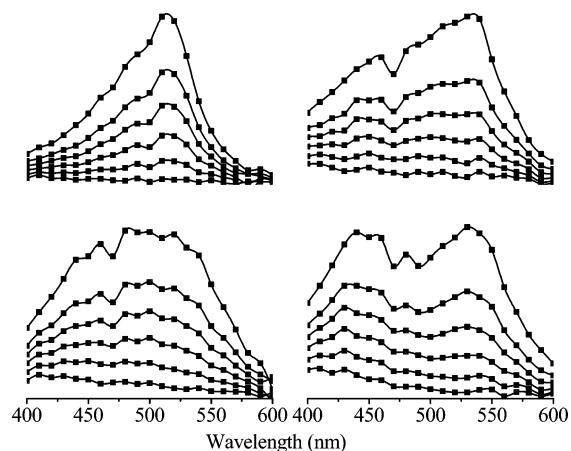


Figure 4. Transient differential absorption spectra recorded for **QT1** (upper left), **QT2** (upper right), **QT3** (lower left), and **QT4** (lower right) in deoxygenated ethanol following excitation with a 4-ns laser pulse at 266 nm. Spectra were recorded at different delay times in the window from 100 ns to 100 μ s, and in each case, the signal decays progressively with increasing delay.

when the optimized geometries for the ground state are used, and for the fluorescence maxima, when the optimized geometries for the S_1 states are used (Table 1). The corresponding triplet energies estimated from low-temperature phosphorescence spectra are around 2.6 eV and are almost insensitive to changes in ground-state geometry. The phosphorescence maxima can be compared to those recorded for biphenyl ($\lambda_P = 450$ nm), terphenyl ($\lambda_P = 490$ nm), and *p*-QP ($\lambda_P = 510$ nm) under the same conditions. The quantum chemical calculations give triplet energies that are much lower than those found at 77 K (Table 1), but this might indicate a geometry change in the glassy matrix. The calculations, however, are consistent with the observed trend in triplet energies.

Transient differential absorption spectra were recorded for **QT1–QT4** in deoxygenated ethanol following excitation at 266 nm with a 4-ns laser pulse. For **QT1**, the spectrum shows a well-defined absorption maximum at 520 nm with evidence for vibrational fine structure at higher energies. This spectrum looks similar to that reported for the parent,⁴⁰ with the absorption maximum for the latter occurring at 525 nm. The transient absorption spectra recorded for the other members of the series are broader and have the appearance of two overlapping peaks of comparable intensity. This is particularly evident for **QT4**, which shows clear maxima at 535 and 445 nm. Decay kinetics are biphasic in each case, and even at relatively low laser power, the triplet state does not decay entirely to the prepulse baseline but leaves a residual absorbance (Figure 4). The residual spectrum is broad and peaks in the near-UV region. The triplet state, which dominates the spectrum, decays via first-order kinetics, and the triplet lifetimes (τ_T) recorded in deoxygenated ethanol at room temperature are given in Table 2. There is a modest variation in τ_T across the series, outside of experimental error, whereby the decay rate seems to decrease as the central dihedral angle increases. The triplet state is quenched by molecular oxygen, and the initial absorbance increases significantly in the presence of iodoethane (10% v/v).

The longer-lived component has an unexceptional differential absorption spectrum that does not resemble that of the *p*-QP π -radical cation formed by photoionization. This latter species is known⁴¹ to absorb around 550 nm. It is likely that the observed species arise from secondary reactions of the π -radical cations with the solvent. Indeed, in deoxygenated acetonitrile at room temperature, transient differential absorption spectra

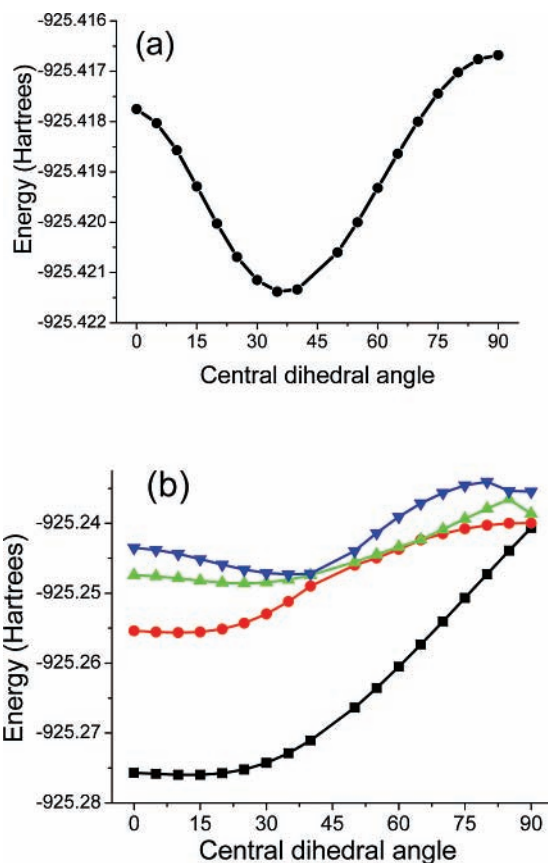


Figure 5. Effect of the central dihedral angle on the computed energies for (a) the ground state and (b) the singlet-excited-state manifold for *p*-QT: S_1 (black), S_2 (red), S_3 (green) and S_4 (blue).

indicate the presence of the π -radical cations in addition to the triplet states. Assuming that the molar absorption coefficient is insensitive to changes in structure, the relative yield of the cation (ϕ_{CAT}) at high laser intensities varies considerably throughout the series (Table 2). There is no real correlation between ϕ_{CAT} and the computed ionization potential (IP) for the molecules in vacuo, for excitation at 266 nm. The polar solvent, however, will lower the energy required to ionize the molecule by a considerable amount,⁴² and there will be a further stabilization because of electrostatic interactions⁴³ with the solvated electron. It is necessary for the S_1 state to absorb a second photon so as to exceed the ionization energy, and there is a reasonable correlation between ϕ_{CAT} and the energy difference between S_1 and the cation, as calculated for the optimized geometries of the two states. It is also notable that ϕ_{CAT} increases proportionally with increasing τ_S , which is consistent with a biphotonic process.⁴⁴ There is a marked decrease in ϕ_{CAT} in the presence of iodoethane, for which τ_S decreases by a factor of about 10.

Spectroscopic Properties. There is, at best, only a tenuous relationship between the optical properties and the computed geometries. That such a correlation should hold can be concluded from examination of Figure 5, in which the effects of rotation about the central C–C bond are shown for *p*-QP. The ground state has a clear energy minimum at around 37°, whereas S_1 prefers a planar geometry and is relatively unstable when the central rings adopt an orthogonal arrangement. The S_2 state also seeks a planar structure, but the angle dependence is less severe than found for S_1 such that the two levels converge at higher angles. The energy of S_3 is less sensitive to changes in the central dihedral angle, but the profile computed for S_4 mirrors that found for the ground state. The net effect is that the energy levels converge at larger angles. It is also important

TABLE 3: Summary of the Properties Derived from Curve Fitting of the Emission Spectra

parameter	T^a (K)	p -QT	QT1	QT2	QT3	QT4
E_{00} (cm ⁻¹)	77	28975	27800	29230	28140	28495
	295	28615	27495	28455	27590	27695
$h\omega_M$ (cm ⁻¹)	77	990	1105	1240	1475	1215
	295	1165	1365	1500	1660	1525
S	77	1.09	0.94	0.86	0.80	0.84
	295	1.08	1.29	1.10	1.01	1.07
E_T (cm ⁻¹)	77					
$h\omega_T$ (cm ⁻¹)	77	1000	1100	1200	1400	1250
S_T	77	1.10	0.95	0.82	0.80	0.83

^a Temperature.

to note that substantial geometric changes are predicted after excitation to both S_1 and S_2 .

For **QT1**, there is only a small change in geometry between the S_0 and S_1 states, and as a consequence, the emission spectrum shows a modest degree of fine structure. The other derivatives undergo a larger geometry change upon excitation, and there is a general increase in the energies of both the S_1 and S_2 states with increasing dihedral angle. The relaxed S_1 geometries are quite similar for all of the compounds, and the preferred dihedral angle is less than that of the corresponding ground state. This leads to a small decrease in the energy of the fluorescent state as the dihedral angle increases and, because of the geometry change on deactivation, a loss of vibrational fine structure. These general effects are retained upon rapid cooling to 77 K, and it appears that the glassy matrix does not inhibit such internal structural changes. The glassy matrix induces a small blue shift of 500 ± 200 cm⁻¹. Similar trends are apparent in the low-temperature phosphorescence spectra, with only **QT1** displaying vibrational fine structure (see Supporting Information). The quantum chemical calculations indicate that the geometries of the energy-minimized T_1 states are remarkably similar to those of the corresponding S_1 states (Table 1). There is, in effect, a clear attempt by the molecule to attain a planar geometry at the lower-lying excited-state level, for both singlet and triplet states.

The fluorescence spectra can be deconvoluted into a series of Gaussian-shaped components of common half-width,⁴⁵ although this is necessarily a crude process, with the highest-energy band (E_{00}) being used to establish the 0,0 energy gap (Table 3). Nonetheless, some interesting features emerge from the analysis. For p -QP, the fluorescence spectrum requires analysis in terms of a series of at least six Gaussian components separated by a medium-frequency vibrational mode ($h\omega_M$) of 990 and 1165 cm⁻¹ at 77 K and room temperature, respectively. Spectra recorded for **QT1** can be analyzed similarly to give $h\omega_M$ modes of 1105 and 1365 cm⁻¹ at 77 K and room temperature, respectively. Again, a long progression of vibronic bands is needed to adequately describe the spectrum,⁴⁵ and it is important to stress that the quality of the fitting routine precludes inclusion of additional low-frequency librations. The remaining spectra, being much broader, could be fit to the sum of four Gaussian components, and the derived $h\omega_M$ modes are compiled in Table 3. Including the parent, there is a marked increase in $h\omega_M$ at the higher temperature and, for the tethered derivatives, an intriguing relationship between $h\omega_M$ and the ground-state dihedral angle, ϕ . The latter effect arises because of angle-dependent variations in the extent of electron delocalization at the ground-state level. Increasing electron delocalization would lower the bond order of aromatic C=C bonds, and thereby decrease the vibrational force constant, but would raise that of the connecting C—C bonds. This would lead to an overall decrease in $h\omega_M$ with increasing delocalization for the accepting

vibration. Because π -electron delocalization is at a maximum when the phenylene rings are coplanar, the observed angle dependence appears to be fully consistent with the computed geometries.

In principle, the phosphorescence spectra could be subjected to the same analysis, but the large slit widths necessary for these latter studies are not conducive to detailed spectral curve fitting. It was noted, however, that the parameters extracted from the phosphorescence spectrum recorded for **QT1** were remarkably similar to those found for the corresponding fluorescence spectrum. Thus, the 0,0 level corresponds to the triplet energy (E_T), and the medium-frequency vibrational mode ($h\omega_T$) coupled to decay of the triplet state has a value of 1100 cm⁻¹ at 77 K (Table 3). The Huang–Rhys factor (S_T) for phosphorescence also remains comparable to that found for fluorescence under the same conditions (Table 3). For the other derivatives, there is a clear relationship between $h\omega_T$ and the computed change in central dihedral angle, and S_T varies in a similar fashion. Such behavior appears to be consistent with the computed geometries for the T_1 states.

The differential triplet–triplet absorption spectra vary throughout the series (Figure 4), changing progressively from a single transition for **QT1** to a broad ensemble of overlapping transitions for **QT4**. The lowest-energy absorption maximum remains at about 520 nm and can be contrasted with those found for terphenyl ($\lambda_{MAX} = 460$ nm) and biphenyl ($\lambda_{MAX} = 365$ nm) under the same conditions. In fact, the transient absorption spectra can be reproduced remarkably well from the computational studies using the calculated oscillator strengths and imposing an arbitrary bandwidth of 50 nm for each transition (Figure 6). These latter studies indicate many new transitions in the near-UV region for the derivatives bearing longer tethers. Such transitions can be accessed because the absolute energies of the lower-lying triplets, notably T_1 and T_2 , depend on ϕ but the energies of the higher-lying triplets are insensitive to changes in this dihedral angle. The net effect is to narrow the relevant energy gaps for the larger ϕ values.

Nonradiative Decay. The rate constants ($k_{RAD} = \phi_F/\tau_S$) for radiative decay of S_1 remain fairly consistent across the series and, within experimental error, can be approximated as 6.4×10^8 s⁻¹ (Table 2). This is a high value but consistent with fluorescence from a ¹L_a excited singlet state.³⁸ In contrast, the corresponding rate constants for nonradiative decay (k_{NR}) from S_1 show a modest dependence on the dihedral angle ϕ . Precisely the same angle dependence is noted for nonradiative decay (k_T) of the triplet excited states in fluid solution (Table 2), which points to a common mechanism. That the orthogonal structure shows the lower rate of decay was quite unexpected and suggests that increased levels of electron delocalization lead to enhanced rate of decay. Within the confines of the energy-gap law,⁴⁶ this effect could be explained in terms of an angle dependence for the Huang–Rhys factor, S ;⁴⁷ the results necessarily require that S decreases with increasing ϕ . This, in fact, turns out to be the case, for both excited singlet and triplet states (Table 3). Thus, the deconvoluted fluorescence spectra can be used to calculate S at both 77 K and room temperature according to the equation

$$I_n = \frac{S^n e^{-S}/n!}{\sum_{m=0}^{\infty} S^m e^{-S}/m!} \quad (1)$$

where I_n is the relative intensity of the n th vibronic peak for a phonon mode of $h\omega_M$ and the denominator normalizes the total

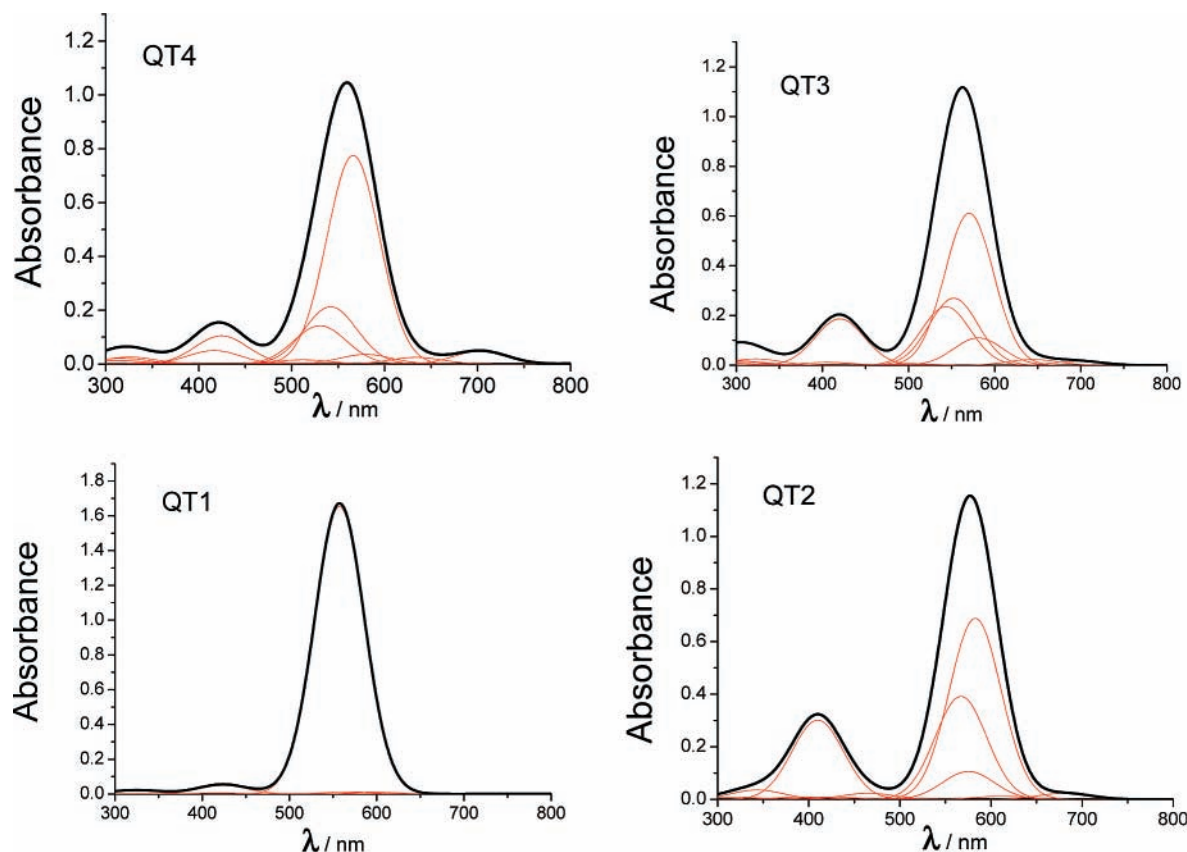


Figure 6. Computed triplet–triplet absorption spectra for the various compounds. The black line represents the overall spectra as compiled by summation of the individual Gaussian components.

intensity to unity.⁴⁸ The same analysis can be applied to the phosphorescence spectra recorded at 77 K. The derived values are included in Table 3. It should be recalled⁴⁹ that this expression is based on two simple harmonic oscillators with displaced equilibrium configurations that leads to a difference in equilibrium potential energy of $\delta = Sh\omega_M$. The energy change is often referred to as the relaxation energy⁴⁸ because δ can be equated to the amount of energy removed by emission of phonons as the system approaches the ground vibrational state.

The outcome of this analysis is that S for the parent compound, where internal rotation is facile, decreases with decreasing temperature because of a change in the degree of exciton delocalization (Table 3). The low-temperature S (or S_T) values derived for the strapped derivatives are somewhat larger than that for *p*-QP and show a small, but definite, dependence on ϕ . The same trend is also observed at room temperature. It is notable that S (or S_T) tends to a minimum as ϕ approaches 90°. Now, S can be expressed as

$$S = \frac{\mu\omega_M}{2\hbar\Delta^2} \quad (2)$$

where μ is the effective reduced mass of the vibrator and Δ is the displacement of the two potential energy surfaces. Assuming that μ remains fixed throughout the series, the variation in S can be satisfactorily explained in terms of the mutual displacement of the potential surfaces. There is, of course, the off-setting effect of ω_M to take into account.

The energy-gap law⁴⁶ can be expressed in terms of eq 3

$$k_{NR} = \frac{2\pi C^2}{h\sqrt{E_{00}}h\omega_M} e^{\gamma} e^{-\gamma(E_{00}/h\omega_M)} \quad (3)$$

where γ is a coefficient that depends on the 0,0 energy gap but

is expected to remain reasonably constant across the series of strapped derivatives. The same equation holds for k_T and is valid as long as the reduced displacement Δ is not too large. The parameter C refers to the electron–vibration coupling matrix element⁴⁸ and will differ markedly for singlet and triplet excited states. According to this expression, the rate constant depends on $h\omega_M$ in both the exponential and pre-exponential terms, and it is known that this parameter increases with increasing strap length, in opposition to S . In a crude sense, changes in the two exponential terms tend to cancel because the absolute magnitude of the angle dependence is roughly the same for both S and $h\omega_M$ (Table 3). The observed changes in k_{NR} and k_T , therefore, are due to alterations in C , as caused by the displacement of the potential surfaces. In other words, changes in the equilibrium geometry of the ground state are responsible for the variations in S , $h\omega_M$, and C and are manifest in the observed rates of nonradiative decay.

Conclusion

The key feature to emerge from this study is that, whereas the S_1 and T_1 geometries tend toward a common value for ϕ of ca. 34°, the geometry of the ground state is effectively set by the length of the tether. The net result is that the rates of nonradiative decay are controlled by the ground-state geometry. Because this geometry influences the extent of electron delocalization, there is a corresponding effect on the magnitude of the medium-frequency vibrational mode coupled to nonradiative decay for both S_1 and T_1 . The resultant displacement of the potential energy surfaces affects the Huang–Rhys factors (i.e., the number of phonons associated with transformation between excited-state and ground-state geometries), and this, in turn, alters the emission spectral profiles. In principle, the changes in geometry that accompany excitation and nonradiative decay

might be expected to cause the decay kinetics to deviate from exponential behavior, but this was not seen in the experiments, even using improved temporal resolution. Interestingly, the length of the tether has little real effect on the energy gaps between the ground state and either S_1 or T_1 but does modify the energy gaps involving higher-lying excited states and thereby perturbs the ionization potential. The rate of nonradiative decay is at a minimum when the ground-state dihedral angle approaches 90° , at least within the limited set of angles available. For both S_1 and T_1 , the rates of nonradiative decay can be approximated by the equation

$$k_{\text{NR}} = k_{\text{IND}} + k_0 \cos^2 \phi \quad (4)$$

where k_0 is the corresponding rate constant for a planar geometry and k_{IND} is an angle-independent rate constant (see Supporting Information). A nonlinear least-squares fit to the (limited) experimental data suggests that there is a 4.6-fold difference in k_{NR} values between the orthogonal and coplanar geometries; the equivalent change for the triplet state is 2.6-fold. In terms of optimizing the performance of a light-emitting diode, these are quite respectable variations in the rate of decay such that this strategy might have useful benefits for the design of improved optical devices. This realization might be amplified by taking into account the full geometry rather than only the central unit.

Acknowledgment. This work was supported by the EPSRC (GR/S00088) and by the University of Newcastle.

Supporting Information Available: Illustration of the bend angle, phosphorescence spectra recorded at 77 K, example of the spectral curve fitting, full listing for ref 25, and plots of nonradiative rate constants versus angle. This material is available free of charge via the Internet at: <http://pubs.acs.org>.

References and Notes

- (1) (a) Lim, S.-H.; Bjorklund, T. G.; Bardeen, C. J. *Chem. Phys. Lett.* **2001**, *342*, 555. (b) Wohlgenannt, M.; Jiang, X. M.; Vardeny, Z. V. *Phys. Rev. B* **2004**, *69*, 241204. (c) Borges, C. A. M.; Marletta, A.; Faria, R. M.; Guimaraes, F. E. G. *Braz. J. Phys.* **2004**, *34*, 590.
- (2) (a) Wohlgenannt, M. *Phys. Status Solidi A: Appl. Res.* **2004**, *201*, 1188. (b) Gartstein, Y. N.; Rice, M. J.; Conwell, E. M. *Phys. Rev. B* **1995**, *52*, 1683. (c) Woo, H. S.; Graham, S. C.; Halliday, D. A.; Bradley, D. D. C.; Friend, R. H.; Burn, P. L.; Holmes, A. B. *Phys. Rev. B* **1992**, *46*, 7379.
- (3) (a) Daminelli, G.; Widany, J.; Di Carlo, A.; Lugli, P. *J. Chem. Phys.* **2001**, *115*, 4919. (b) Demanze, F.; Cornil, J.; Garnier, F.; Horowitz, G.; Valat, P.; Yasser, A.; Lazzaroni, R.; Brédas, J. L. *J. Phys. Chem. B* **1997**, *101*, 4553. (c) Kanemitsu, Y.; Suzuki, K.; Masumoto, Y.; Tomiuchi, Y.; Shiraiishi, Y.; Kuroda, M. *Phys. Rev. B* **1994**, *50*, 2301.
- (4) (a) Beljonne, D.; Wittmann, H. F.; Köhler, A.; Graham, S.; Younus, M.; Lewis, J.; Raithby, P. R.; Khan, M. S.; Friend, R. H.; Brédas, J. L. *J. Chem. Phys.* **1996**, *105*, 3868. (b) Monkman, A. P.; Burrows, H. D.; Hamblett, I.; Navarathnam, S.; Svensson, M.; Andersson, M. R. *J. Chem. Phys.* **2001**, *115*, 9046. (c) Janssen, S. W.; Blatchford, J. W.; Lin, L. B.; Gustafson, T. L.; Partee, J.; Shinar, J.; Fu, D. K.; Marsella, M. J.; Swager, T. M.; MacDiarmid, A. G.; Epstein, A. J. *Synth. Met.* **1997**, *84*, 501.
- (5) (a) Oliveira, F. A. C.; Cury, L. A.; Righi, A.; Moreira, R. L.; Guimaraes, P. S. S.; Matinaga, F. M.; Pimenta, M. A.; Nogueira, R. A. *J. Chem. Phys.* **2003**, *119*, 9777. (b) Cornil, J.; Beljonne, D.; dos Santos, D. A.; Shuai, Z.; Brédas, J. L. *Synth. Met.* **1996**, *78*, 209.
- (6) Casado, J.; Hicks, R. G.; Hernandez, V.; Myles, D. J. T.; Ruiz Delgado, M. C.; Lopez-Navarrete, J. T. *J. Chem. Phys.* **2003**, *118*, 1912.
- (7) Weiss, E. A.; Tauber, M. J.; Kelley, R. F.; Ahrens, M. J.; Ratner, M. A.; Wasielewski, M. R. *J. Am. Chem. Soc.* **2005**, *127*, 11842.
- (8) (a) Correia, H. M. G.; Barbosa, H. M. C.; Ramos, M. M. D. *J. Non-Cryst. Solids* **2006**, *352*, 1691. (b) Bruschi, M.; Giuffreda, M. G.; Luthi, H. P. *Chem. Eur. J.* **2002**, *8*, 4216. (c) Liang, W. Z.; Zhao, Y.; Sun, J.; Song, J.; Hu, S. L.; Yang, J. L. *J. Phys. Chem. B* **2006**, *110*, 9908. (d) Toudic, B.; Limelette, P.; Froyer, G.; Le Gac, F.; Moreac, A.; Rabiller, P. *Phys. Rev. Lett.* **2005**, *95*, 215502. (e) Blatchford, J. W.; Gustafson, T. L.; Epstein, A. J. *J. Chem. Phys.* **1996**, *105*, 9214. (f) Bai, X.; Holdcroft, S. *Macromolecules* **1993**, *26*, 4457. (g) Aubert, P. H.; Beouch, L.; Tran-Van, F.; Stephan, O.; Chevrot, C. *Synth. Met.* **2006**, *156*, 898.
- (9) (a) Schwab, P. F. H.; Smith, J. R.; Michl, J. *Chem. Rev.* **2005**, *105*, 1197. (b) Rodriguez, J. G.; Lafuente, A.; Rubio, L. *Tetrahedron Lett.* **2004**, *45*, 5685. (c) Ng, S. C.; Ong, T. T.; Chan, H. S. O. *J. Mater. Chem.* **1998**, *8*, 2663.
- (10) (a) Anariba, F.; Steach, J. K.; McCreery, R. L. *J. Phys. Chem. B* **2005**, *109*, 11163. (b) Venkataraman, L.; Klare, J. E.; Nuckolls, C.; Hybertsen, M. S.; Steigerwald, M. L. *Nature* **2006**, *442*, 904. (c) Donhauser, Z. J.; Mantooth, B. A.; Kelly, K. F.; Bumm, L. A.; Monnell, J. D.; Stapleton, J. J.; Price, D. W., Jr.; Rawlett, A. M.; Allara, D. L.; Tour, J. M.; Weiss, P. S. *Science* **2001**, *292*, 2303.
- (11) (a) Berlin, Y. A.; Hutchinson, G. R.; Rempala, P.; Ratner, M. A.; Mich, J. *J. Phys. Chem. A* **2003**, *107*, 3970. (b) Emberley, E.; Kirzenow, G. *Phys. Rev. Lett.* **2003**, *91*, 188301. (c) Moresco, F.; Meyer, G.; Rieder, K. H.; Tang, H.; Gourdan, A.; Joachim, C. *Phys. Rev. Lett.* **2001**, *86*, 672. (d) Dulic, D.; van der Molen, S. J.; Kudernac, T.; Jonkman, H. T.; de Jong, J. J.; Borden, T. N.; van Esch, J.; Feringa, B. L.; van Wees, B. J. *Phys. Rev. Lett.* **2003**, *91*, 207402. (e) Yasuda, S.; Nakamura, T.; Matsumoto, M.; Shigekawa, H. *J. Am. Chem. Soc.* **2003**, *125*, 16430.
- (12) Benniston, A. C.; Harriman, A.; Li, P. Y.; Patel, P. V.; Sams, C. A. *J. Org. Chem.* **2006**, *71*, 3481.
- (13) Benniston, A. C.; Harriman, A.; Li, P. Y.; Sams, C. A.; Ward, M. D. *J. Am. Chem. Soc.* **2004**, *126*, 13630.
- (14) Benniston, A. C.; Harriman, A.; Li, P. Y.; Patel, P. V.; Sams, C. A. *Phys. Chem. Chem. Phys.* **2005**, *7*, 3677.
- (15) Benniston, A. C.; Harriman, A.; Li, P. Y.; Patel, P. V.; Rostron, J. P.; Sams, C. A. *J. Phys. Chem. A* **2006**, *110*, 9880.
- (16) (a) Berlman, I. B. *J. Phys. Chem.* **1970**, *74*, 3085. (b) Berlman, I. B.; Wirth, H. O.; Steingraber, O. J. *J. Phys. Chem.* **1971**, *75*, 318. (c) Berlman, I. B. *J. Phys. Chem.* **1973**, *77*, 562.
- (17) (a) Tousey, R.; Limansky, I. *Appl. Opt.* **1972**, *11*, 1025. (b) Nogue, J. L.; Majewski, S.; Walker, J. K.; Bowen, M.; Wojcik, R.; Moreshead, W. V. *J. Am. Ceram. Soc.* **1988**, *71*, 1159.
- (18) Gundlach, D. J.; Lin, Y. Y.; Jackson, T. N.; Schlom, D. G. *Appl. Phys. Lett.* **1997**, *71*, 3853.
- (19) (a) Corney, A.; Manners, J.; Webb, C. E. *Opt. Commun.* **1979**, *31*, 354. (b) Zuev, V. S.; Logunov, O. A.; Savinov, Y. V.; Startsev, A. V.; Stoilov, Y. Y. *Appl. Phys.* **1978**, *17*, 321.
- (20) Taber, R. L.; Daub, G. H.; Hayes, F. N.; Ott, D. G. *J. Heterocycl. Chem.* **1965**, *2*, 181.
- (21) Simpson, J. E.; Daub, G. H.; Hayes, F. N. *J. Org. Chem.* **1973**, *38*, 4428.
- (22) Perrin D. D.; Armarego, W. L. F. *Purification of Laboratory Chemicals*, 3rd ed.; Pergamon Press Ltd.: Oxford, U.K., 1988.
- (23) Morris, J. V.; Mahoney, M. A.; Huber, J. R. *J. Phys. Chem.* **1976**, *80*, 969.
- (24) Schmidt, M. W.; Baldrige, K. K.; Boatz, J. A.; Elbert, S. T.; Gordon, M. S.; Jensen, J. J.; Koseki, S.; Matsunga, N.; Nguyen, K. A.; Su, S.; Windus, T. L.; Dupuis, M.; Montgomery, J. A. *J. Comput. Chem.* **1993**, *14*, 1347.
- (25) Frisch et al. *Gaussian 03*; Gaussian, Inc.: Pittsburgh, PA, 2003. See Supporting Information for a full listing.
- (26) Foresman, J. B.; Head-Gordon, M.; Pople, J. A.; Frisch, M. J. *J. Phys. Chem.* **1992**, *96*, 135.
- (27) (a) Champagne, B.; Mosley, D. H.; Fripiat, J. G.; Andre, J. M. *Phys. Rev. B* **1996**, *54*, 2381. (b) Lavrentiev, M. Y.; Barford, W. *J. Chem. Phys.* **1999**, *111*, 11177. (c) Miao, M. S.; Van Camp, P. E.; Van Doren, V. E.; Ladik, J. J.; Mintmire, J. W. *J. Chem. Phys.* **1998**, *109*, 9623.
- (28) Stephens, P. J.; Devlin, F. J.; Chabrowski, C. F.; Frisch, M. J. *J. Phys. Chem.* **1994**, *98*, 11623.
- (29) Bauschlicher, C. W., Jr.; Partridge, H. *J. Chem. Phys.* **1995**, *103*, 1788.
- (30) (a) Head-Gordon, M.; Rico, R. J.; Oumi, M.; Lee, T. J. *J. Chem. Phys. Lett.* **1994**, *219*, 21. (b) Head-Gordon, M.; Maurice, D.; Oumi, M. *J. Phys. Chem. Lett.* **1995**, *246*, 114.
- (31) Foresman, J. B.; Frisch, A. *Exploring Chemistry with Electronic Structure Methods*; 2nd ed.; Gaussian Inc.: Pittsburgh, PA, 1996.
- (32) (a) Jamorski, C.; Casida, M. E.; Salahub, D. R. *J. Chem. Phys.* **1996**, *104*, 5134. (b) Bauernschmitt, R.; Ahlrichs, R. *Chem. Phys. Lett.* **1996**, *256*, 454. (c) Bauernschmitt, R.; Häser, M.; Treutler, O.; Ahlrichs, R. *Chem. Phys. Lett.* **1997**, *264*, 573. (d) Hirata, S.; Head-Gordon, M. *Chem. Phys. Lett.* **1999**, *314*, 291.
- (33) Benniston, A. C.; Harriman, A.; Li, P. Y.; Sams, C. A. *Tetrahedron Lett.* **2003**, *44*, 4167.
- (34) Franzén, R. *Can. J. Chem.* **2000**, *78*, 957.
- (35) (a) Cailleau, H.; Baudour, J. L.; Zeyer, C. M. E. *Acta Crystallogr. B* **1979**, *35*, 426. (b) Stumber, M.; Zimmermann, H.; Schmidt, H.; Haebleren, U. *Mol. Phys.* **2001**, *99*, 1091.
- (36) (a) Delugeard, Y.; Desuche, J.; Baudour, J. L. *Acta Crystallogr. B* **1976**, *32*, 702. (b) Baudour, J. L.; Cailleau, H.; Yelan, W. B. *Acta Cryst.*

tallogr. B **1977**, 33, 1773. (c) Baudour, J. L.; Delugeard, H.; Rivet, P. *Acta Crystallogr. B* **1978**, 34, 625.

(37) Akiyama, M.; Watanabe, T.; Kakihana, M. *J. Phys. Chem.* **1986**, 90, 1752.

(38) Birks, J. B. *Photophysics of Aromatic Molecules*; Wiley-Interscience: London, 1970.

(39) (a) Nijegorodov, N. I.; Mabbs, R. *Spectrochim. Acta A* **2002**, 58, 349. (b) Nijegorodov, N. I.; Downey, W. S.; Danailov, M. B. *Spectrochim. Acta A* **2000**, 56, 783. (c) Mabbs, R.; Nijegorodov, N. I.; Downey, W. S. *Spectrochim. Acta A* **2003**, 59, 1329.

(40) Pavlopoulos, T. G.; Hammond, P. R. *J. Am. Chem. Soc.* **1974**, 96, 6568.

(41) Bennema, P.; Hoijsink, G. J.; Lupinski, J. H.; Oosterhoff, L. J.; Selier, P.; van Voorst, J. D. W. *Mol. Phys.* **1959**, 2, 431.

(42) Watkins, A. R. *J. Phys. Chem.* **1976**, 80, 713.

(43) Grand, D.; Bernas, A. *J. Phys. Chem.* **1977**, 81, 1209.

(44) Piciulo, P. L.; Thomas, J. K. *J. Chem. Phys.* **1978**, 68, 3260.

(45) (a) Guha, S.; Rice, J. D.; Yau, Y. T.; Martin, C. M.; Chandrasekhar, M.; Chandrasekhar, H. R.; Guetner, R. *Phys. Rev. B* **2003**, 67, 125204. (b) Lim, E. C.; Li, Y. H. *J. Chem. Phys.* **1970**, 52, 6416.

(46) Englman, R.; Jortner, J. *Mol. Phys.* **1970**, 18, 145.

(47) Bassler, H.; Schweitzer, B. *Acc. Chem. Res.* **1999**, 32, 173.

(48) (a) Kennedy, S. P.; Garro, N.; Phillips, R. T. *Phys. Rev. B* **2000**, 64, 115206. (b) Di Bartolo, B.; Powell, R. C. *Phonons and Resonance in Solids*; Wiley: New York, 1976.

(49) (a) Hagler, T. W.; Pakbaz, K.; Voss, K. F.; Heeger, A. J. *Phys. Rev. B* **1991**, 44, 8652. (b) Beljonne, D.; Shuai, Z.; Friend, R. H.; Brédas, J. L. *J. Chem. Phys.* **1995**, 102, 2042. (c) Shuai, Z.; Brédas, J. L.; Su, W. P. *Chem. Phys. Lett.* **1994**, 228, 301. (d) Cornil, J.; Beljonne, D.; Heller, C. M.; Campbell, I. H.; Laurich, B. K.; Smith, D. D. C.; Bradley, K.; Mullen, K.; Brédas, J. L. *Chem. Phys. Lett.* **1997**, 278, 139.